Mechanical activation and non-local rheology in granular flows

Bouzid Mehdi, Martin Trulsson, Philippe Claudin, Eric Clément, and Bruno Andreotti
Physique et Mécanique des Milieux Hétérogènes, UMR 7636 ESPCI – CNRS – Univ. Paris-Diderot – Univ. P.M. Curie, 10 rue Vauquelin, 75005 Paris, France

(Dated: January 16, 2013)

Based on the idea that the motion of an assembly of rigid particles is mostly determined by the volume fraction, we propose a non-local constitutive relation for dense granular flows. This rheology is tested against discrete element simulations and calibrated using the spatial relaxation of the rheology observed under a homogeneous stress. We show that the creep flow obtained below yield conditions is quantitatively described by the same liquid rheology as the shear flow obtained above yield conditions. In the spirit of the experiment of Reddy *et al.* [1], we investigate the influence of a shear band far away from the studied zone on its mechanical behaviour. The dominant features of the experiment are recovered both in the numerical simulations and in the analytical model. The later quantitatively fits the numerical data without any adjustable parameter.

Granular materials belong to the class of amorphous athermal systems. Like foams [2, 3], emulsions [4], suspensions [5–7] or metallic glasses [8], they exhibit a dynamical phase transition between *static* and *flowing* states. Analogously to phase transitions of thermodynamic systems, this *jamming* transition exhibits a divergence of correlation lengths [9–11], revealing the presence of non-local cooperative processes called dynamical heterogeneities [12]. In order to describe the constitutive behavior of such systems, it is therefore natural to adopt the Ginzburg-Landau phenomenological approach of phase transitions [11, 13–15]. The main issue is then to identify the relevant control and order parameters. Following the now classical Liu-Nagel diagram for jamming transition [16], it is usually assumed that the *solid-liquid mechanical transition* is controlled by the shear stress τ [11, 14, 15], which, once rescaled by its critical value, defines the yield parameter $\mathcal{Y}$. For a granular system under a fixed confining pressure P, one gets a Coulomb criterion $\mathcal{Y} = \mu_c^{-1}\,\tau/P$, where μ_c is the dynamical yield friction coefficient. The order parameter is then the shear rate $\dot\gamma$ or any combination of $\dot\gamma$ and the stress components, like the fluidity $\dot\gamma/\tau$. However, different experiments have challenged this Coulomb picture, which assumes a transition between solid ($\dot\gamma = 0$) and liquid ($|\dot\gamma| > 0$) states at $\mathcal{Y} = 1$. (i) In the inclined plane geometry, thin granular layers flow anomalously [17] and stop at a yield parameter $\mathcal{Y} > 1$ [18, 19]. (ii) A creeping flow is commonly observed in regions which are expected to be jammed, since $\mathcal{Y} < 1$. [19–21] (iii) A solid plunged in grains and submitted to a force lower than the yield threshold starts moving as soon as a shear band is created far away from the solid [1, 22]. Moreover, from the mechanical point of view, the choice of $\mathcal{Y}$ as a control parameter suffers from a major flaw: the stress is not amongst the state variables. Indeed, following Newton's law, the state of the system is determined by the particles positions and velocities, from which forces are deduced. To say it differently, a dynamical phase transition model based on the assumption that the stress field is known cannot be introduced in continuum dynamical equations to extend Navier-Stokes to yield stress fluids. To do so, one needs a formulation where stresses are *deduced* from true state variables: volume fraction, strain, strain rate, coordination number, fabric tensor, etc. The aim of this letter is to propose a phenomenology for dense granular flows and to test it against discrete element simulations.

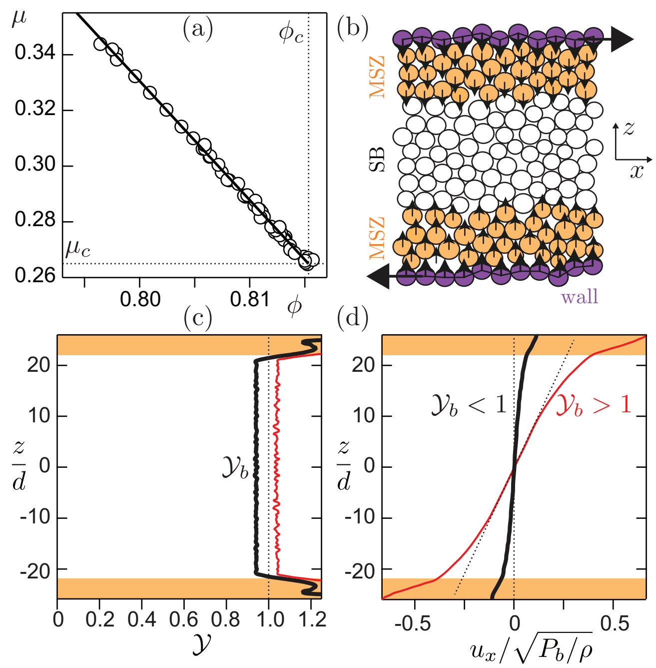

FIG. 1: (Color online) (a) Relation between the effective friction coefficient μ and the volume fraction ϕ. (b) Schematic of the numerical set-up used to calibrate spatial relaxation to the bulk constitutive relation. (c) Typical profiles of the yield parameter $\mathcal{Y}$ obtain numerically below (thick black line, $|\mathcal{Y}_b| < 1$) and above (thin red line, $|\mathcal{Y}_b| > 1$) yield conditions. (d) Corresponding velocity profiles. The dotted lines show the predictions of a local rheology. P_b is the pressure in SB.

Before proceeding to the derivation of the non-local rheology, we wish to emphasize that Ginzburg-Landau approach does not capture much (if anything) from the dynamical mechanisms at work, which (unfortunately)

constitute a separate issue. The stress-based approach implicitly assumes that a flow can be decomposed into a quasi-static sequence of plastic events. In this picture, localized plastic rearrangements get triggered when the *local* stress state crosses a microscopic *local* yield criterion [11, 23, 24] , namely, a local Coulomb criterion in the case of granular matter. These localized events induce long-range fluctuations of the stress over the system, which can "activate" a cascade of new plastic events. The mechanical fluctuations in amorphous athermal systems would then play the role of temperature in thermal systems: rearrangements would be *mechanically activated*, suggesting a picture analogous to Eyring's transition state theory for the viscosity of liquids [1, 23]. The shear rate $\dot{\gamma}$ then gives the rate at which quasi-static realizations of the contact force network are generated.

This *kinetic elastoplastic* picture is challenged by the *geometrical* picture, which has been developed for disordered packings of particles that interact through repulsive contact forces. In this alternative approach, mechanical properties are related to the contact network geometry and to the distance to isostaticity [9, 25–27]. It has been recently shown that the statistical properties of grain trajectories and in particular their cooperative non-affine motions are mostly controlled by the volume fraction ϕ, whatever the nature of the dissipative mechanisms [28]. To move by a distance as the crow flies equal to its diameter d, a grain makes a random-like motion whose average length diverges as $\sim d(\phi_c - \phi)^{-1}$, leading to a stress tensor diverging as $f(\phi) \sim (\phi_c - \phi)^{-2}$ [6, 7, 28]. Provided the flow is homogeneous, the stress ratio τ/P is related to the volume fraction ϕ by a function $\mu(\phi)$ (Fig. 1a) which does not depend on the interparticle friction coefficient nor on the flow regime (overdamped or inertial) [7]. In this geometrical picture, the "local plastic events" are replaced by "non-local cooperative motions"; the ability to flow is governed by steric effects and controlled by the volume fraction in the *neighborhood* of the particle.

Following the geometrical picture, the lowest order correction to a local rheology [19, 29] involves the parameter

$$\kappa \equiv -d^2 \frac{\nabla^2 \phi}{\phi_c - \phi}, \tag{1}$$

when the linearity and the isotropy of the response to a variation of ϕ is assumed. The rheology of a dense inertial granular flow can then be written under the form:

$$\frac{\sigma_{ij}}{\rho d^2} = -f(\phi)|\dot{\gamma}|^2 \delta_{ij} + (1 - \chi(\kappa))\, f(\phi)\mu(\phi)|\dot{\gamma}|\dot{\gamma}_{ij} \tag{2}$$

where $\dot{\gamma}_{ij} = \left(\frac{\partial u_i}{\partial x_j} + \frac{\partial u_j}{\partial x_i}\right)$ is the rate of strain tensor and ρ the density. χ is the non-local correction, which verifies $\chi(\kappa) \simeq \chi'_0 \kappa + \mathcal{O}(\kappa^2)$ (Fig. 2b). κ is positive when the point considered is surrounded by a lower volume-fraction: the shear stress therefore decreases. For a simple shear, the volume fraction can be eliminated between

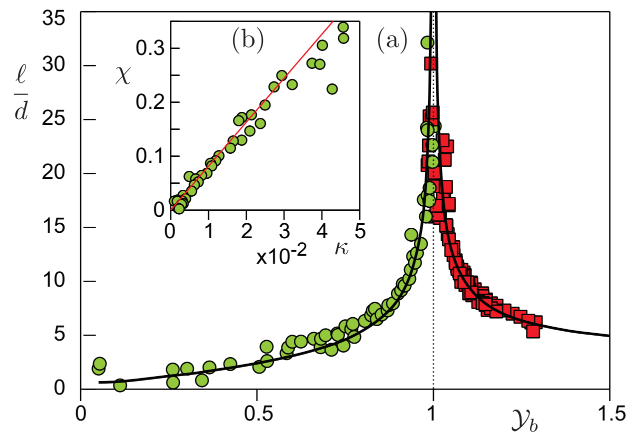

FIG. 2: (Color online) (a) Relaxation length ℓ below ($\circ$) and above ($\square$) yield conditions. The solid line is a phenomenological fit to the data that diverges as $|\mathcal{Y}_b - 1|^{-1/2}$. (b) Function $\chi(\kappa)$ measured for $\mathcal{Y}_b < 1$. The red solid line shows the slope $\chi'_0 \simeq 8$ deduced from the best fit of the data for $\mathcal{Y}_b > 1$.

the shear stress $\tau = \sigma_{xz}$ and the pressure $P = -\sigma_{zz}$. The non-local rheology can then be expressed as: $|\mathcal{Y}| = (1 - \chi(\kappa))\, \mu(\phi)/\mu_c$. However, formaly as $\mu(\phi)$ and $I(\phi)$ are linear [30], the very same non-local rheology can be expressed in terms of the inertial number $I = |\dot{\gamma}| d/\sqrt{P/\rho}$ rather than ϕ, to match the kinetic elastoplastic picture. I compares the rate at which plastic event occurs $\sim |\dot{\gamma}|$ to the inertial time-scale $\sim d/\sqrt{P/\rho}$ over which these events take place. One gets:

$$|\mathcal{Y}| = \frac{\mu(I)}{\mu_c}\,(1 - \chi(\kappa)) \quad \text{and} \quad \kappa = d^2 \frac{\nabla^2 I}{I}. \tag{3}$$

In both formulations, we consider that the whole granular assembly flows, *whatever the yield parameter* $\mathcal{Y}$, as soon there is a flow somewhere. The very same rheology then applies to fast flows, above the yield criterion $\mathcal{Y} > 1$, and to evanescent flows, below the yield criterion $\mathcal{Y} < 1$.

We have calibrated and tested this non-local rheology using molecular dynamics simulations (see [30] for details). The system is two-dimensional and slightly polydisperse. Contacts are frictional. The shear cell is composed by two rough walls, with periodic boundary conditions along the direction x parallel to the walls (Fig. 1b). The position of the walls is controlled to ensure a constant normal stress and a constant velocity. We consider the limit of rigid grains for which results do not depend any longer on the microscopic spring constant nor on the damping time. The originality of the numerical set-up is the presence of bulk forces applied to the grains, which depend of their positions (Fig. 1b). The system behaves as if there was gravity field varying in space. The bulk forces can be either along z, to vary P, or along x, to vary τ. We are therefore able to impose the field of $\mathcal{Y}$, once the system as reached a steady state (Fig. 1c).

We first impose homogeneous stress conditions in the center of the shear cell (noted SB for shear band in

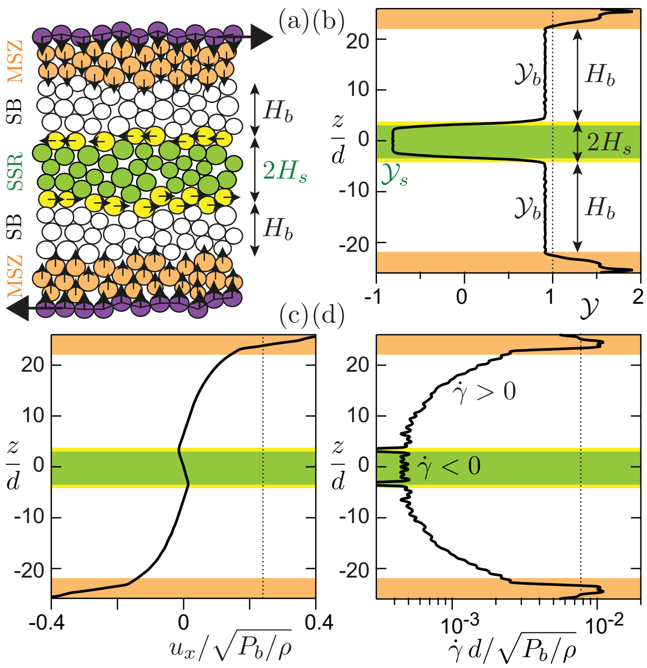

FIG. 3: (Color online) a) Schematic of the numerical set-up used to investigate non-local effects. (b) Typical profile of the yield parameter $\mathcal{Y}$. (c) Velocity profile. (d) Velocity gradient profile. P_b is the pressure in both SB and SSR.

Fig. 1b). The later is surrounded by two buffer zones hereafter called the *master shear zones* (MSZ) and in which $\mathcal{Y}$ is gradually varied using vertical forces (Fig. 1c). One observes that the velocity profile in the central zone is not linear but is well fitted by the form $\dot\gamma_b z + C\ \sinh(z/\ell)$ as predicted by the linearization of Eq. (2) around the bulk inertial number (Fig. 1d). Above yielding conditions, the predicted relaxation length ℓ reads

$$\ell = d\sqrt{\frac{|\mathcal{Y}_b|\chi_0'}{|\mathcal{Y}_b|-1}} \quad \text{for} \quad |\mathcal{Y}_b| > 1 \tag{4}$$

while below yielding conditions, one gets $\dot\gamma_b = 0$ and

$$\ell = \frac{d}{\sqrt{\chi^{-1}\left(1-|\mathcal{Y}_b|\right)}} \quad \text{for} \quad |\mathcal{Y}_b| < 1 \tag{5}$$

Therefore, the relaxation length ℓ should diverge symmetrically on both sides of the yielding condition $|\mathcal{Y}_b| = 1$, as $\sim d\sqrt{\chi_0'}\ \left||\mathcal{Y}_b|-1\right|^{-1/2}$. Fig. 2a shows that this relation is nicely verified by the data. Let us emphasize again that both sides of the divergence correspond to the liquid granular state and are predicted by the very same non-local correction $\chi(\kappa)$. For $|\mathcal{Y}_b| < 1$ the grains in the SB only flow due to the influence of the MSZ, which are above yielding conditions. Importantly, the existence of a linear response of the system around the critical state ($I = 0$ and $\phi = \phi_c$) imposes to build κ by rescaling $\nabla^2\phi$ by $\phi_c - \phi$ (or $\nabla^2 I$ by I, Eq. 7).

We now carry out a numerical experiment similar in principle to that performed by Reddy *et al* [1] in a Couette cell. The conceptual idea is to measure the rheology in the shear band, which is below yield conditions, under the influence of the master shear zone (MSZ) located close to the rigid boundaries. To implement such a *slaved secondary rheometer* (SSR), the shear stress is changed in a small region of width $2H_s$ around the center of the shear cell, by applying horizontal forces to the grains (Fig. 3). It is characterized by the yield parameter $\mathcal{Y}_s$ and by the central shear rate $\dot\gamma_s$. The flow in the SSR is slaved to that forced in the MSZ, which is characterized by a shear rate $\dot\gamma_m$. The SSR is separated from the MSZ by a region of width H_b characterized by a yield parameter $0 < \mathcal{Y}_b < 1$. So, there is a single observable, $\dot\gamma_s$ and five parameters: $\dot\gamma_m$, $\mathcal{Y}_b$, H_b, $\mathcal{Y}_s$ and H_s.

Experimentally, the SSR used in [1] is a small immersed rod submitted to an external force, which, once rescaled by its critical value, plays the role of $\mathcal{Y}_s$. The rod creep velocity is the analogous of $\dot\gamma_s$. The shear rate $\dot\gamma_m$ of the MSZ is controlled by the rotation velocity of the inner cylinder. Note that contrarily to the numerical set-up, the radial profile of the yield parameter $\mathcal{Y}$ is inhomogeneous in the Couette cell. The three key observations reported in [1] are recovered here. (i) The shear rate $\dot\gamma_s$ in the SSR is proportional to the shear rate $\dot\gamma_m$ in the MSZ (Fig. 4a). (ii) $\dot\gamma_s$ (roughly) decreases exponentially with the distance to the yield conditions in the SSR, measured by $1-|\mathcal{Y}_s|$. (Fig. 4a) (iii) $\dot\gamma_s$ decreases exponentially with H_b (Fig. 4b). In [1], the property (i) has been interpreted as the signature of a quasi static flow and (ii) as a Boltzmann-like factor suggesting an Eyring-like mechanical activation. This Boltzmann-like factor was itself related in [23] to the exponential tail of the contact force distribution, using the kinetic elastoplastic approach.

Can the three properties shared by the experiment and the numerics be recovered in the non-local formalism derived here? Using again the linearization of Eq. 2 around the critical state, the solution in the SSR takes the form $\dot\gamma = \dot\gamma_s\ \cosh\left[z/\ell(\mathcal{Y}_s)\right]$ while in the SB, it reads $\dot\gamma = \dot\gamma_+\ \exp\left[z/\ell(\mathcal{Y}_b)\right] + \dot\gamma_-\ \exp\left[-z/\ell(\mathcal{Y}_b)\right]$. At the interface $z = H_s$ of the secondary rheometer, the model predicts that $|\dot\gamma|$ is continuous *even when* $\dot\gamma$ *changes sign.* This property is remarkably verified in the numerics (Fig. 3d). Matching $|\dot\gamma|$ at $z = H_s$, one gets

$$\frac{\dot\gamma_m}{|\dot\gamma_s|} = \left[\cosh\left(\frac{H_s}{\ell(\mathcal{Y}_s)}\right) + \frac{\ell(\mathcal{Y}_b)}{\ell(\mathcal{Y}_s)}\sinh\left(\frac{H_s}{\ell(\mathcal{Y}_s)}\right)\right]\exp\left(\frac{H_b}{\ell(\mathcal{Y}_b)}\right)$$

in the limit $H_b \gg \ell(\mathcal{Y}_b)$. This expression is reported in Fig. 4 without any adjustable parameter. The agreement with the numerical points is almost perfect when the SSR is sheared in the direction opposite to the MSZ ($\mathcal{Y}_s < 0$).

The non-local model predicts the proportionality of $\dot\gamma_s$ and $\dot\gamma_m$ (property i) as a trivial consequence of the linearization of the rheological equation. It explicitly predicts that the influence of the distance H_b can be factorized and is exponential (property iii), due to the spatial

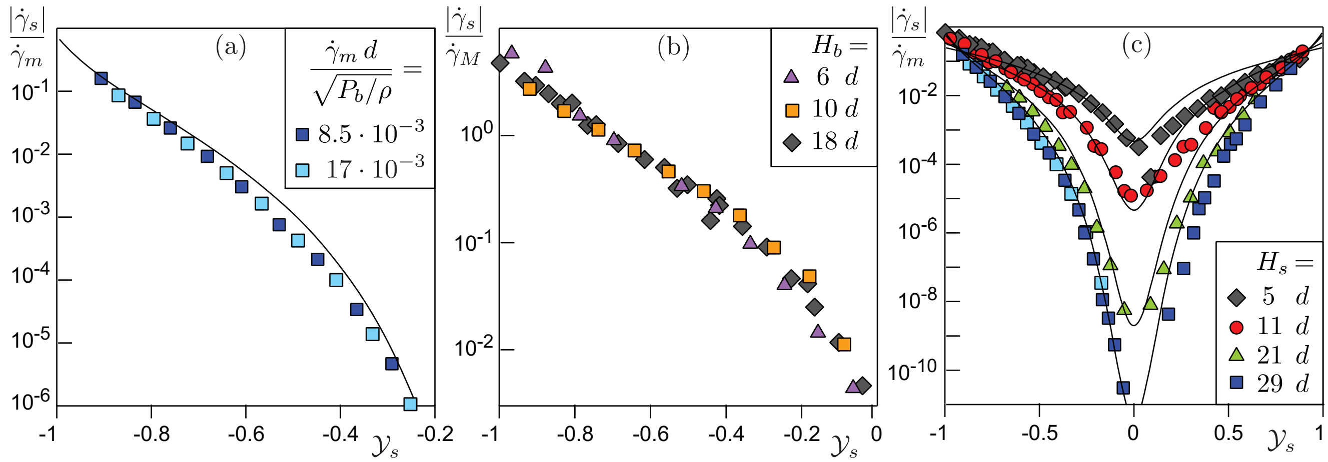

FIG. 4: (Color online) Ratio of the shear rate in the secondary rheometer $\dot\gamma_s$ to that in the master shear band $\dot\gamma_m$. (a) Linearity of the response. (b) Data obtained for different distances H_b collapse on a master curve, once rescaled by the factor giving the influence of the distance: $\dot\gamma_M = \dot\gamma_m \, \exp\left(-H_b/\ell(\mathcal{Y}_b)\right)$. (c) Influence of the size H_s of the secondary rheometer. The solid lines are the predictions of the non-local rheology obtained without any adjustable parameter.

relaxation of $\dot\gamma$ in the zone separating the SSR from the MSZ. The fast exponential-like decay of $\dot\gamma_s$ with $1-|\mathcal{Y}_s|$ (property ii) also results from the spatial relaxation of the shear rate, but this time inside the SSR.

Our results demonstrate that the granular material constitute a single liquid phase across yielding conditions ($\mathcal{Y}=1$), which continuously connects the fast shear flow (MSZ) to the evanescent flow in the secondary rheometer (SSR), even when the direction of the flow is reversed (continuity of $|\dot\gamma|$). The three properties shared by the experiment, by the numerics, and by the analytics turn out to be simple consequences of the linearization around the critical state. Exponential factors are therefore neither associated to Boltzmann factors nor to the tails of the contact force probability distribution function, as previously assumed. Finally, Fig. 4c shows a blind prediction that can be easily tested experimentally, although not reported in [1]. One observes that the size of the SSR ($\sim$ the rod) has a strong influence on $\dot\gamma_s$ ($\sim$ the creep velocity): the wider the SSR, the faster the decay of $\dot\gamma_s$ with the distance to yield conditions. The non-local rheology proposed here must now be included into Navier-Stokes solvers to test its predictions in more demanding geometries like the split-bottom setup or the channelized avalanches, as well as for time-dependent flows.

[1] K. A. Reddy, Y. Forterre, and O. Pouliquen, Phys. Rev. Lett. **106**, 108301 (2011).

[2] F. Bolton and D. Weaire, Phys. Rev. Lett. **65**, 3449 (1990).

[3] A. Kabla and G. Debrégeas, Phys. Rev. Lett. **90**, 258303 (2003)

[4] M. Clusel, E.I. Corwin, A.O.N. Siemen and J. Brujic, Nature. **460**, 611 (2009) .

[5] C. Bonnoit, T. Darnige, E. Clément, and A. Lindner, J. Rheol. **54**, 65 (2010)

[6] F. Boyer, E. Guazzelli, and O. Pouliquen, Phys. Rev. Lett. **107**, 188301 (2011)

[7] M. Trulsson, B. Andreotti, and P. Claudin, Phys. Rev. Lett. **109**, 118305 (2012).

[8] S. Xie and E.P. George, Acta Mater. **56**, 5202 (2008).

[9] M. Wyart, S. R. Nagel, and T. A. Witten, Europhys. Lett. **72**, 486 (2005).

[10] C. Heussinger, L. Berthier, and J.-L. Barrat, Europhys. Lett. **90**, 20005 (2010).

[11] L. Bocquet, A. Colin,and A. Ajdari, Phys. Rev. Lett. **103**, 036001 (2009).

[12] O. Dauchot, D.J. Durian, M. van Hecke, in ”Dynamical heterogeneities in glasses, colloids, and granular media”, (Oxford University Press) (2011).

[13] Aranson, I. S. and Tsimring, L. S. Rev. Mod. Phys. 78, 641692 (2006).

[14] J. Goyon, A. Colin, G. Ovarlez, A. Ajdari, and L. Bocquet, Nature. **454**, 84 (2008).

[15] K. Kamrin and G. Koval Phys. Rev. Lett. 108, 178301 (2012).

[16] Liu, A. J. and Nagel, S. R. Nature. **396**, 21-22 (1998).

[17] S. Deboeuf, E. Lajeunesse, O. Dauchot and B. Andreotti, Phys. Rev. Lett. **97**, 158303 (2006).

[18] Pouliquen, O. Phys. Fluids. **11**, 542-548 (1999).

[19] GDR MiDI, Eur. Phys. J. E. **14**, 341 (2004).

[20] T. S. Komatsu, S. Inagaki, N. Nakagawa, and S. Nasumo, Phys. Rev. Lett. 86, 1757 (2001).

[21] V.B Nguyen, T.Darnige, A. Bruand, E. Clement, Phys. Rev. Lett. **107**, 138303 (2011)

[22] K. Nichol *et al.* Phys. Rev. Lett. 104, 078302 (2010).

[23] O. Pouliquen, Y. Forterre, Phil. Trans. R. Soc. A. 367, 5091-5107 (2009).

[24] P. Sollich *et al* Phys. Rev. Lett. **78**, 2020 (1997); P. Hébraud and F. Lequeux Phys. Rev. Lett. **81**, 2934 (1998);

[25] M. van Hecke, J. Phys.: Cond. Matt. **22**, 033101 (2010)

[26] B. P. Tighe *et al.* Phys. Rev. Lett. **105**, 088303 (2010)

[27] E. Lerner, G. Düring and M. Wyart, Proc. Natl. Acad. Sci. USA **109** 47984803 (2012).

[28] B. Andreotti, J.-L. Barrat, and C. Heussinger, Phys. Rev. Lett. **109**, 105901 (2012).

[29] P. Jop, Y. Forterre, and O. Pouliquen, Nature. **441**, 727 (2006).

[30] Supplemental Material

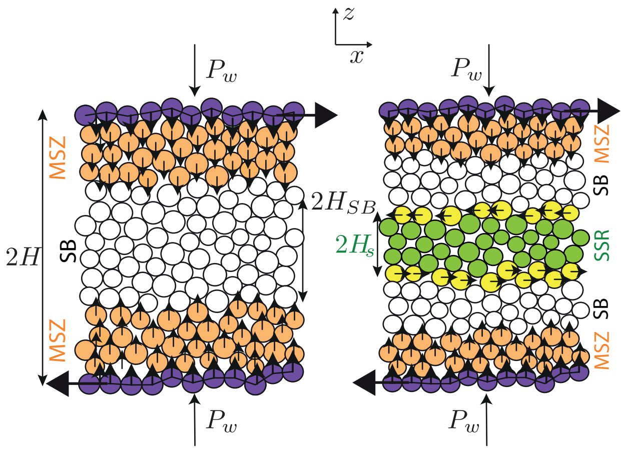

FIG. 5: a) Schematics of the simulation set-up. Walls are depicted by dark purple circles. (b) Same, but now also with the secondary rheometer illustrated.

SUPPLEMENTAL MATERIAL

Numerical model and viscoelastic parameters

We consider a two-dimensional system constituted of $\simeq 2 \cdot 10^3$ circular particles of mass m_i and diameter d_i, with a ± 20 % polydispersity (Fig. 5). The shear cell is composed of two rough walls distant by H and each moving along the x-direction at different constant velocities, with the difference of the velocities equal to u_x^{wall}. The position of the walls is controlled to ensure a constant normal stress P_w at the walls (whereby H will change/fluctuate during the simulations). Periodic boundary conditions are applied along x. The particle and wall dynamics is integrated using the Verlet algorithm. The particles are submitted to contact forces modeled as viscoelastic forces along the normal direction and as a Coulomb friction along the tangential direction [1–3].

The normal spring constant k_n is chosen sufficiently large (i.e. $k_n/P > 10^3$) to reach the rigid asymptotic regime. The Coulomb friction coefficient is chosen equal to $\mu_p = 0.4$ and damping parameters are chosen such to yield a restitution coefficient $e \simeq 0.9$.

External forces and the second rheometer

In order to create a zone below the yield condition (i.e. $|\mathcal{Y}| < 1$), two anti-directional vertical gravity-like forces were applied on the grains with gaussian spatial distributions (on particle labelled i):

$$f_z^i(z_i) = \hat{f}_z m_i \Big(\exp\Big[-\frac{(z_i-\delta_t)^2}{2\sigma^2} \Big] - \exp\Big[-\frac{(z_i-\delta_b)^2}{2\sigma^2} \Big] \Big)$$

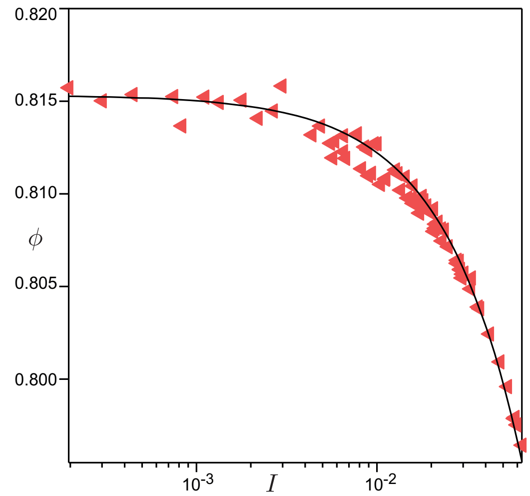

FIG. 6: The volume fraction ϕ as a function of the inertial number I. Numerical data points are given by triangles and Eq. 6 by the solid line.

Where the origin of the z-axis is taken in the center of the cell, $\delta_t = (H - H_{SB})$ and $\delta_b = (H_{SB} - H)$, $\sigma \simeq d$ and $\hat{f}_z$ is the magnitude of the forcing.

We furthermore introduced a second (stress controlled) rheometer in our simulation set-up. This was done by applying two horizontal anti-directional stresses within the zone below yield conditions separated a distance $2H_s$ apart. The second rheometers imposed forces were given by distributing a stress over a horizontal layer of grains on respectively sides of the entrance of the second rheometer (as illustrated in Fig. 1).

Analytical solution

The local rheology of a granular flow is given by,

$$\phi(I) = \phi_c - \alpha I \quad \text{and} \quad \mu(\phi) = \mu_c\big(1 + \beta(\phi_c - \phi)\big). \quad (6)$$

For the specific system with the values $\phi_c = 0.8153$, $\mu_c = 0.2665$, $\alpha = 0.3112$, and $\beta = 15.6127$ (see Fig. 2 in the SI and Fig. 1a in the Letter).

The nonlocal rheology in terms of the inertial number I (analogous derivation can be written in terms of the volume fraction ϕ) is given by (Eq. 3 in the Letter):

$$|\mathcal{Y}| = \frac{\mu(I)}{\mu_c}\,(1 - \chi(\kappa)) \quad \text{and} \quad \kappa = d^2 \frac{\nabla^2 I}{I}, \quad (7)$$

where χ is the non-local correction, which to a first approximation reads $\chi(\kappa) \simeq \chi_0'\kappa + \mathcal{O}(\kappa^2)$. We first consider the situation above yielding conditions $|\mathcal{Y}| > 1$. Linearizing the equations around the zero order $|\mathcal{Y}| = 1 + \beta I_0$, where I_0 is the local approximation, one gets:

$$I_1 - \frac{\chi\prime_0 |\mathcal{Y}|}{|\mathcal{Y}| - 1} d^2 \nabla^2 I_1 = 0. \quad (8)$$

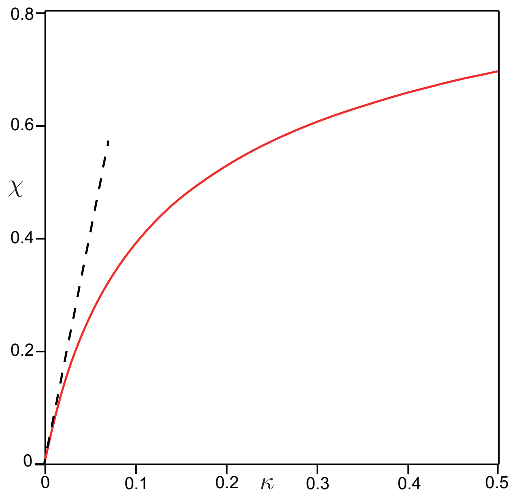

FIG. 7: *Red solid line*: The full nonlocal correction χ as a function of κ according to Eq. 10. *Black dashed line*: Linear approximation of Eq. 6 (i.e. $\chi = \chi_0'\kappa$ and with $\chi_0' = 8$).

The solution I_1 (i.e. the non-local correction to the inertial number) takes the form $\sim \cosh(z/\ell)$ with $\ell = d\sqrt{\frac{\chi_0'|\mathcal{Y}|}{|\mathcal{Y}|-1}}$.
Below the yielding condition $|\mathcal{Y}| < 1$ we instead linearize the equations around the critical state $I_0 = 0$ and find:

$$|\mathcal{Y}| = 1 - \chi(\kappa) \quad \text{or} \quad \chi^{-1}(1 - |\mathcal{Y}|) = d^2 \frac{\nabla^2 I_1}{I_1}. \tag{9}$$

Once again one finds that I_1 is given on the form $\sim \cosh(z/\ell)$, but now with $\ell = \frac{d}{\sqrt{\chi^{-1}(1-|\mathcal{Y}|)}}$.
For small κ (i.e. close to the yield condition $|\mathcal{Y}| = 1$) the length ℓ is found to be well approximated by $\sim d\sqrt{\chi_0'}\ ||\mathcal{Y}_b| - 1|^{-1/2}$. For larger κ and below the yield condition we, however, found that the non-local function χ took the shape (see Fig. 3):

$$\chi = \frac{\sqrt{(1-\kappa a)^2 + \kappa b(\kappa a - 1)}}{a\kappa - 1} + 1, \tag{10}$$

with $a = -15.95$ and $b = 16.3$. This gives rise to an asymmetry in ℓ around $|\mathcal{Y}| = 1$ when sufficiently far away from the same point (as seen in Fig. 2 in the Letter).

[1] F. da Cruz, S. Emam, M. Prochnow, J. N. Roux, and F. Chevoir, Phys. Rev. E **72**, 021309 (2005).

[2] P. A. Cundall and O. D. L. Strack, Geotechnique **29**, 47 (1979).

[3] S. Luding, Behavior of Granular Media, 137-147, Shaker Verlag, Aachen (2006).